Reliable Attribute-missing Multi-view Clustering with Instance-level and Feature-level Cooperative Imputation

Anonymous Authors

ABSTRACT

Multi-view clustering (MVC) constitutes a distinct approach to data mining within the field of machine learning. Due to limitations in the data collection process, missing attributes are frequently encountered. However, existing MVC methods primarily focus on missing instances, showing limited attention to missing attributes. A small number of studies employ the reconstruction of missing instances to address missing attributes, potentially overlooking the synergistic effects between the instance and feature spaces, which could lead to distorted imputation outcomes. Furthermore, current methods uniformly treat all missing attributes as zero values, thus failing to differentiate between real and technical zeroes, potentially resulting in data over-imputation. To mitigate these challenges, we introduce a novel Reliable Attribute-Missing Multi-View Clustering method (RAM-MVC). Specifically, feature reconstruction is utilized to address missing attributes, while similarity graphs are simultaneously constructed within the instance and feature spaces. By leveraging structural information from both spaces, RAM-MVC learns a high-quality feature reconstruction matrix during the joint optimization process. Additionally, we introduce a reliable imputation guidance module that distinguishes between real and technical attribute-missing events, enabling discriminative imputation. The proposed RAM-MVC method outperforms nine baseline methods, as evidenced by real-world experiments using single-cell multi-view data.

CCS CONCEPTS

• **Computing methodologies** → **Cluster analysis**; • **Theory of computation** → **Unsupervised learning and clustering**;

KEYWORDS

Multi-view Clustering, Multi-view Learning, Attribute-missing Imputation

1 INTRODUCTION

Multi-view clustering (MVC) represents a pivotal paradigm in machine learning, garnering widespread attention owing to its superior performance in uncovering data structures [7, 13, 33, 50, 54]. By aggregating information from multiple views, MVC offers a comprehensive understanding of the data and is extensively applied across a variety of real-world scenarios [10, 16, 22, 41, 45, 57], including biomedical research, social network analysis, and recommendation systems, etc. However, due to technical limitations of collection equipment, complex system environments, and privacy concerns, missing attributes in multi-view data remain a prevalent issue [1, 8]. For instance, within the public biological dataset [2], over 80% of the collected multi-modal sequencing results for various genes are missing, as is illustrated in Fig. 1. The missing attributes pose a significant challenge to existing MVC analysis.

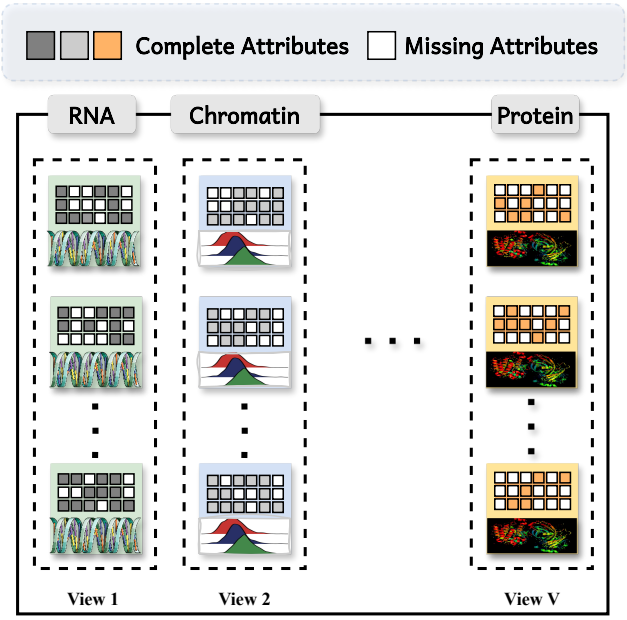

Figure 1: Multi-view data exhibiting missing attributes, as exemplified in biomedical scenarios.

Existing MVC methods predominantly address issues of instance-level missingness [18, 20, 21, 23], referring to incomplete instances within the observed view. Several studies introduce the concept of view-level missingness [12, 25, 39, 43], which is just a specific case of instance-level missingness that occurs when all samples in a view are missing. These studies typically develop a mapping function between complete and missing views to impute zero values in missing instances. For instance, Goeleven et al. developed separate mapping functions for each of the four complete views to impute information in target views with missing samples [11]. These mappings are constructed based on instance-level similarity, neglecting feature similarity and thus overlooking potential synergies between instance and feature spaces. Furthermore, in real-world multi-view data, cases of missing attributes occur far more frequently than those of missing instances. For example, in patients undergoing physical examinations, data on respiratory function, blood pressure, and electrocardiograms were collected,

Unpublished working draft. Not for distribution.

ACM MM, 2024, Melbourne, Australia

ACM ISBN 978-x-xxxx-xxxx-x/YY/MM
https://doi.org/10.1145/nnnnnnn.nnnnnnn

while urine tests were inadvertently omitted. Existing MVC methods fail to account for missing attributes and are neither effective nor appropriate for addressing the attribute-missing issue. Merely applying the mapping function learned in the instance space for imputation can lead to distorted outcomes.

Furthermore, existing MVC methods address missing attributes indiscriminately [5, 38, 48, 52, 53, 56]. However, in practical applications, there are at least two scenarios for missing attributes: real and technical zero values. For instance, one student genuinely scored zero points on an exam, while another earned ninety-nine points but was assigned a score of zero due to the loss of his test paper. Non-discriminatory restoration of zero values can result in students who genuinely scored zero points receiving inflated scores, deviating from actual outcomes. This problem is especially prevalent in biomedical contexts. Single-cell multi-view data frequently feature a significant number of zero values [17, 26, 30]. Some of these zero values signify expression intensities with biological significance, whereas others stem from information loss attributable to technical detection limitations. Indiscriminate imputation can lead to unexpected and uninterpretable outcomes.

To address the aforementioned issues, we have developed a novel MVC framework for handling missing attributes, named Reliable Attribute-Missing Multi-View Clustering (RAM-MVC). This model comprises two main modules: 1) A reliable imputation guidance module, which assesses whether imputation should proceed based on the confidence levels of zero values and discriminates between real and technical zero values. 2) A bi-level cooperative imputation module that simultaneously extracts structural information from both feature and instance spaces, thereby enhancing the feature reconstruction process. Fig. 2 depicts the architecture of the proposed RAM-MVC framework. The contributions of this study are summarized as follows:

- We propose a pioneering unified attribute-missing MVC framework that seamlessly integrates bi-level imputation with reliable guidance, ensuring both components collaborate effectively to achieve accurate imputation and enhanced clustering performance.
- The developed imputation guidance module effectively differentiates between real and technical attribute-missing events, thus addressing the over-imputation problem prevalent in existing MVC methods. Additionally, by leveraging the structural information from both the instance and feature spaces, the Bi-level imputation module jointly optimizes the feature reconstruction matrix and secures high-quality features.
- An effective alternative optimization algorithm is designed to solve the proposed RAM-MVC model. Extensive experimental results demonstrate the model's superiority over other benchmark methods.

2 RELATED WORK

During the data collection process, a significant portion of multi-view data often experiences the loss of specific views or values due to technical limitations. The MVC method seeks to leverage the consistency and complementarity of features across multiple views to address the missing data, thus mitigating the impact of incomplete data on clustering performance. In this section, we will categorize and review the existing missing MVC methods into two types: Instance-missing MVC Methods and Attribute-missing MVC Methods.

2.1 Instance-missing MVC Methods

In terms of instance absence, Liu et al. redefined the issue of missing instances as a challenge of completing incomplete view similarity graphs [28], successfully yielding discriminative representations. Zhang et al. introduced a two-step strategy that combines missing view imputation with hidden view learning to develop an interpretable model [55]. Wang et al. formulated a completion module leveraging cross-view relation transfer to infer missing data via graph networks [42]. Xu et al. introduced a mixed Gaussian prior and proposed a new strategy based on variational autoencoders, effectively aggregating information from multiple views and optimizing shared representation, thereby achieving improved clustering performance [46]. Additionally, Chao et al. proposed a novel incomplete contrastive multi-view clustering method recently. They utilized an attention mechanism to fuse samples and employed confidence levels to learn complementary information between each view. Furthermore, an end-to-end framework was designed to integrate multiple steps for joint optimization [6]. Liu et al. proposed an instance-level similarity graph learning method to enhance existing incomplete MVC methods [29]. They compressed all instances into a shared space, constructed cross-view similarities, and continuously optimized the constructed similarity matrix. This approach achieved excellent results in addressing the incomplete multi-view clustering challenge.

2.2 Attribute-missing MVC Methods

Regarding attribute absence, Peng et al. employed graph diffusion techniques to enhance the consistency of node embeddings across two views [35], thus facilitating attribute imputation within the input space of graphs. However, their method remains operational at the instance level, without the ability to modify attribute values. Pu et al. developed an adaptive imputation layer for handling missing multi-view data [36]; the layer constructs upon the results of soft clustering across multiple views, and is integrated with global cluster centroids. Nonetheless, it primarily addresses missing instances. Yu et al. introduced the concept of value-level missing. They performed a simple matrix correction to allow the existing MVC method to be applicable for incomplete MVC data, but did not delve into further research on missing attributes [51]. Different from these methods, Wu et al.'s team constructed a generative adversarial model based on optimal transmission theory to enhance the interpolation process [44]. This interpolation method was proven effective, yet further exploration of the clustering framework was not pursued. Despite these advancements, no multi-view clustering model has been specifically designed to address missing attributes. Furthermore, current methods neglect the potential synergistic effects between the instance and feature spaces.

3 PROPOSED METHOD

First, we provide a brief introduction to the mathematical notations used in our manuscript. The multi-view data comprises n instances across v views and can be mathematically represented

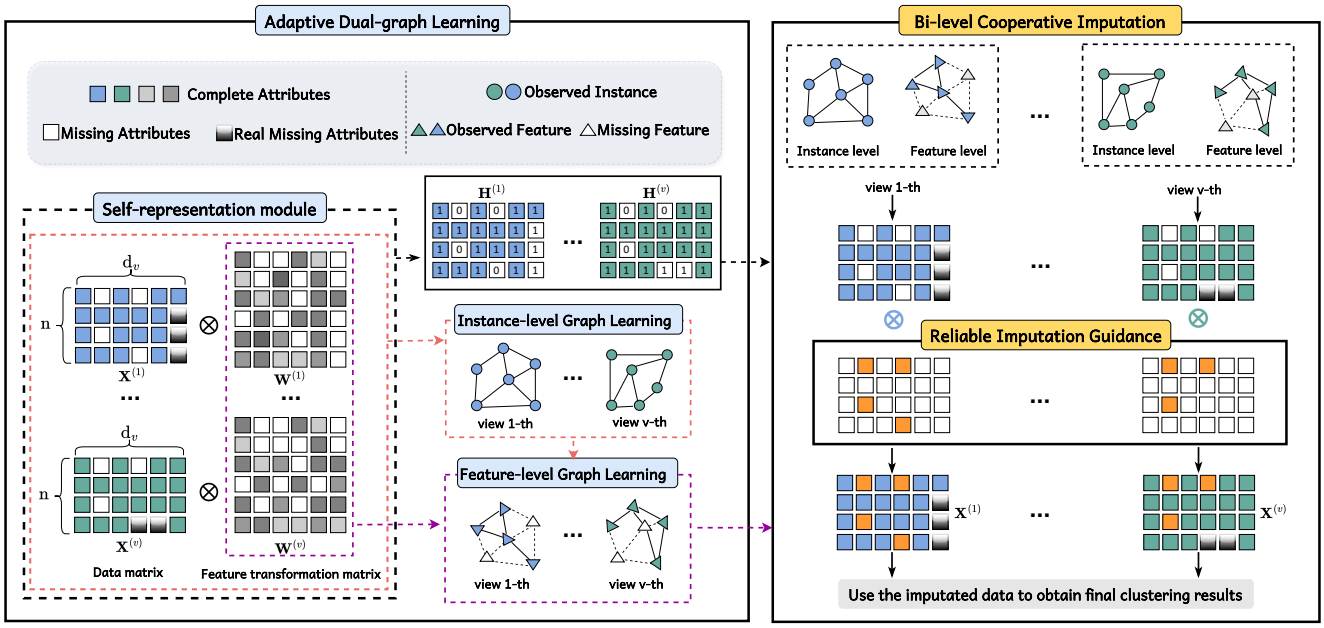

Figure 2: The framework for the proposed RAM-MVC. This model is composed of two main modules: 1) A Reliable Imputation Guidance Module that distinguishes between real and technical missing events during the imputation process. 2) A Bi-Level Cooperative Imputation Module that reconstructs features based on structural information from both the instance and feature spaces.

Table 1: Symbol Appointment

Symbol	Description
d_p	The dimension in the p-th view.
N	The number of the instances.
$z_j^{(k)}$	The zero expression rate in the k-th cluster.
$m_j^{(k)}$	The mean value in the k-th cluster.
$q_j^{2(k)}$	The variance value in the k-th cluster.
$l_j^{(k)}$	The confidence level of zero value.
$\mathbf{X}^{(p)} \in \mathbb{R}^{n\times d_p}$	The raw data of the p-th view.
$\mathbf{H}^{(p)} \in \mathbb{R}^{n\times d_p}$	The reliable imputation guidance matrix of the p-th view.
$\mathbf{W}^{(p)} \in \mathbb{R}^{d_p\times d_p}$	The feature transforming matrix of the p-th view.
$\mathbf{S} \in \mathbb{R}^{n\times n}$	The similarity matrix.
$\mathbf{L}_s \in \mathbb{R}^{n\times n}$	The Laplacian matrix.
$\cdot^\top$	The transpose of matrix.
$\|\|\cdot\|\|_F$	Frobenius norm.
$\mathrm{Tr}(\cdot)$	The trace of matrix.
α_p	The weight coefficient of the p-th view.
λ	Regularization parameters.
t	Confidence threshold.

as $\{\mathbf{X}^{(p)} \in \mathbb{R}^{n\times d_p}\}_{p=1}^{v}$, where $\mathbf{X}^{(p)} = \{\mathbf{x}_1^{(p)}; ...; \mathbf{x}_n^{(p)}\}$, and d_p denotes the dimension in the p-th view. The Frobenius norm of $\mathbf{X}^{(p)}$ is expressed as $\|\mathbf{X}^{(p)}\|_F = \sqrt{\sum_{i=1}^{n}\sum_{j=1}^{d_p}(x_{ij}^{(p)})^2}$, while $\mathrm{Tr}(\mathbf{X}^{(p)})$ and $\mathbf{X}^{(p)\top}$ respectively represent the trace and transpose of $\mathbf{X}^{(p)}$. Symbols used in our paper can be referenced in Table 1.

3.1 Reliable Imputation Guidance Module

There are two potential types of attribute-missing events: 1) Real missing events, which refer to the non-expression of features in instances, resulting in zero values, and 2) Technical missing events, which refer to the loss of attributes during the data collection process due to limitations of technologies. Here, we aim to retain the real missing events as they provide insights into real-world facts, while recovering the technical zero values to address the information loss.

To differentiate between these two types of attribute missingness, confidence levels for each feature $l_j^{(k)}$ are computed according to scImpute [19]. Specifically, zero values for features exhibiting high expression and low variability within instance clusters are considered technical zeros and require recovery. Conversely, features that consistently exhibit low levels of expression and demonstrate high variability are identified as real zeros, reflecting important insight and requiring preservation. The formula for calculating the confidence levels $l_j^{(k)}$ is provided below:

$$l_j^{(k)} = \frac{\left(1 - z_j^{(k)}\right) m_j^{(k)}}{\left(1 - z_j^{(k)}\right) m_j^{(k)} + z_j^{(k)} q_j^{2(k)}}, \tag{1}$$

where k represents the cluster number, while $z_j^{(k)}$, $m_j^{(k)}$, and $q_j^{2(k)}$ denote the zero expression rate, the mean value, and the variance value, respectively.

The reliable imputation guide matrix $\mathbf{H}$ is computed based on the confidence levels $l_j^{(k)}$. The process is as follows:

$$h_{ij} = \begin{cases} 1 & \text{if } x_{ij} > 0, \\ 1 & \text{if } l_j^{(k)} < t \in (0,1), \\ 0 & \text{otherwise.} \end{cases} \tag{2}$$

where t denotes the confidence threshold established to prevent excessive imputation. Guiding matrix $\mathbf{H}$ corresponds in dimensions to the numerical matrix $\mathbf{X}$, with elements populated exclusively by values of 0 and 1. These indicate whether missing values should be imputed at corresponding locations in $\mathbf{X}$. If the confidence level falls below t, a value in matrix $\mathbf{H}$ is set to 1, thus protecting the real zero values from imputing.

3.2 Feature-level Graph Learning

When missing features appear in the observed view, utilizing existing features to infer the missing ones represents a simple and intuitive idea. Therefore, we propose extending the concept of self-representation to the feature level. Specifically, we posit that each feature can be reconstructed via a linear combination of other features. Given the multi-view dataset $\mathbf{X}^{(p)} \in \mathbb{R}^{n \times d_p}$, we present the mathematical formulation as follows:

$$\min_{\mathbf{W}^{(p)\top}\mathbf{W}^{(p)}=\mathbf{I}} \sum_{p=1}^{v} \|\mathbf{X}^{(p)} - \mathbf{X}^{(p)}\mathbf{W}^{(p)}\|_F^2, \tag{3}$$

where $\mathbf{W}^{(p)} \in \mathbb{R}^{d_p \times d_p}$ denotes the projection matrix for the p-th view, used to map the original data to a new feature space. Each row in $\mathbf{W}^{(p)}$ signifies the contribution of each feature to the reconstruction, relative to other features. In essence, this matrix can illustrate the significance of each feature. Furthermore, orthogonal constraints $\mathbf{W}^{(p)\top}\mathbf{W}^{(p)} = \mathbf{I}$ are applied to $\mathbf{W}^{(p)}$ to promote feature independence, helping to eliminate redundant information among features. Moreover, limiting the complexity of the transformation matrix will constrain the model's capacity, thereby mitigating the risk of overfitting. In this study, we employ the matrix $\mathbf{W}^{(p)}$ to facilitate the reconstruction of missing features, thus, the quality of the reconstructed features is deeply contingent upon the quality of $\mathbf{W}^{(p)}$.

3.3 Instance-level Graph Learning

Numerous MVC methods focus on feature recovery by reconstructing instance-level information, with their limitations outlined in our prior discussion. However, these limitations should not be interpreted as a disregard for the importance of the structural information in the instance space. We maintain that structural information in both instance and feature spaces is of equal importance. Their joint optimization facilitates the capture of potential synergistic effects across domains, enabling the model to uncover deeper insights into the missing data. Therefore, in this section, we introduce the construction of structural information at the instance level.

Leveraging the foundational principles of spectral theory and manifold learning [9], the similarity between two instances in the original high-dimensional space signifies their proximity within a specific local neighborhood in that space. Consequently, this similarity ought to be preserved during the dimensional reduction of these data to a lower-dimensional space. In light of the aforementioned principles, we have devised a module to adaptively learn the nearest neighbor graph and obtain the structural information of the instance space, with the corresponding formula expressed as follows:

$$\begin{aligned} &\min_{\mathbf{S}} \sum_{i,j=1}^{n} \|\mathbf{x}_{i,:}^{(p)}\mathbf{W}^{(p)} - \mathbf{x}_{j,:}^{(p)}\mathbf{W}^{(p)}\|_2^2 s_{ij}, \\ &\text{s.t. } s_{ij} \geq 0, \mathbf{1}^\top \mathbf{s}_{:,i} = 1, \end{aligned} \tag{4}$$

where $\mathbf{x}_{i,:}^{(p)}$ denotes the i-th row of $\mathbf{X}^{(p)}$, while $\mathbf{x}_{:,i}^{(p)}$ denotes the i-th column of $\mathbf{X}^{(p)}$. The constraints $s_{ij} \geq 0$ guarantee the rationality of the constructed similarity matrix, while the column constraints of $\mathbf{1}^\top \mathbf{s}_{:,i} = 1$ ensure that the elements of each column in the similarity matrix sum to 1, preventing single data points from disproportionately influencing the overall structure.

To facilitate a simpler solution, leveraging the properties of matrix trace, Eq. (4) can be transformed into an equivalent form for optimization:

$$\begin{aligned} &\min_{\mathbf{S}} \operatorname{Tr}\left(\mathbf{W}^{(p)\top}\mathbf{X}^{(p)\top}\mathbf{L}_\mathbf{S}\mathbf{X}^{(p)}\mathbf{W}^{(p)}\right), \\ &\text{s.t. } \mathbf{S} \geq 0, \mathbf{1}^\top \mathbf{S} = \mathbf{1}, \end{aligned} \tag{5}$$

where $\mathbf{L}_\mathbf{S} = \mathbf{I} - \mathbf{D}^{-\frac{1}{2}}\mathbf{S}\mathbf{D}^{-\frac{1}{2}}$ represents the Laplacian matrix, $\mathbf{S}$ represents the similarity matrix, and $\mathbf{D}$ represents the diagonal matrix derived from $\mathbf{S}$.

3.4 Bi-level Cooperative Imputation

Instance-level similarity has been extensively utilized in feature reconstruction and has achieved widespread verification [40, 49], whereas interpreting feature-level similarity presents challenges. To provide an intuitive understanding, we use single-cell multi-view data as an example, which regards genes as features and highlights a complex network of interactions among genes.

Therefore, we posit that structural information concurrently exists within both instance and feature spaces, and these two spaces possess the potential for synergistic effects. To adaptively learn the structural information from both the instance and feature spaces, we combine Eq. (3) and Eq. (5) to construct the bi-level objective function as follows:

$$\begin{aligned} &\min_{\mathbf{W}^{(p)},\mathbf{S},\boldsymbol{\alpha}} \sum_{p=1}^{V} \|\mathbf{X}^{(p)} - \mathbf{X}^{(p)}\mathbf{W}^{(p)}\|_F^2 + \\ &\sum_{p=1}^{V} \alpha_p^2 \operatorname{Tr}\left(\mathbf{W}^{(p)\top}\mathbf{X}^{(p)\top}\mathbf{L}_\mathbf{S}\mathbf{X}^{(p)}\mathbf{W}^{(p)}\right) + \lambda\|\mathbf{S}\|_F^2, \\ &\text{s.t. } \mathbf{W}^{(p)\top}\mathbf{W}^{(p)} = \mathbf{I}, \mathbf{S} \geq 0, \mathbf{1}^\top \mathbf{S} = \mathbf{1}, \boldsymbol{\alpha} \geq 0, \boldsymbol{\alpha}^\top \mathbf{1} = 1, \end{aligned} \tag{6}$$

where α_p denotes the weight coefficient of the p-th view, which is constructed to balance individual views. By optimizing Eq. (6), we can effectively learn the structural information at both the instance and feature levels, thus obtaining a more accurate $\mathbf{W}^{(p)}$. As we state in Section 3.2, the quality of the reconstructed features is deeply contingent upon the quality of $\mathbf{W}^{(p)}$. By enhancing the quality of $\mathbf{W}^{(p)}$, we ultimately obtain the high-quality reconstructed feature.

Algorithm 1 Iterative Algorithm of RAM-MVC

Input: Attribute-miss multi-view data $\{\mathbf{X}^{(p)}\}_{p=1}^{v}$; the parameters α and λ; the threshold of imputation guidance t.

Initialize $\{\mathbf{W}^{(p)}\}_{p=1}^{v}$, $\boldsymbol{\alpha}$, and $\mathbf{S}$.
Calculate $\mathbf{H}^{(p)}$ via Eq. (2).
while not convergent **do**
  Update $\{\mathbf{W}^{(p)}\}_{p=1}^{v}$ via Algorithm 2;
  Update $\mathbf{S}$ by solving Eq. (13);
  Update $\boldsymbol{\alpha}$ by solving Eq. (16);
end while
Calculate $\{\hat{\mathbf{X}}^{(p)}\}_{p=1}^{v}$ via Eq. (7);
Calculate $\hat{\mathbf{S}}$ by solving Eq. (8);

Output: Perform spectral clustering on $\hat{\mathbf{S}}$ to obtain the final results.

Algorithm 2 Algorithm of updating $\mathbf{W}^{(p)}$

Initialize $\mathbf{W}^{(p)*} = \mathbf{W}^{(p)}$.
while not convergent **do**
  $\mathbf{B}^{(p)} = 2\left(\gamma_{max}\mathbf{I} - \mathbf{A}^{(p)}\right)\mathbf{W}^{(p)*} + 2\mathbf{X}^{(p)\top}\mathbf{X}^{(p)}$;
  Perform SVD on $\mathbf{B}^{(p)}$ as $\mathbf{B}^{(p)} = \mathbf{U}^{\top}\Sigma\mathbf{V}$;
  $\mathbf{W}^{(p)*} = \mathbf{U}^{\top}\mathbf{V}$;
end while
Output: $\mathbf{W}^{(p)} = \mathbf{W}^{(p)*}$.

After obtaining high-quality reconstructed features, we refrain from directly imputing them into the corresponding missing features. As previously mentioned, this operation leads to over-imputation issues. Here, we employ the guiding matrix $\mathbf{H}$ to perform discriminatory imputation. The imputation process is computed as follows:

$$\hat{\mathbf{X}}^{(p)} = (\mathbf{1} - \mathbf{H}^{(p)}) \circ \mathbf{X}^{(p)}\mathbf{W}^{(p)} + \mathbf{X}^{(p)}, \tag{7}$$

where $\circ$ represents the Hadamard product, $\hat{\mathbf{X}}^{(p)}$ represents the data after imputation, embodying high-quality features and subsequently utilized for further clustering analysis. Specifically, we recompute the similarity as follows:

$$\begin{aligned} &\min_{\hat{\mathbf{S}}} \sum_{p=1}^{V}\sum_{i,j=1}^{n} \|\hat{\mathbf{x}}_{i,:}^{(p)} - \hat{\mathbf{x}}_{j,:}^{(p)}\|_2^2 \hat{s}_{ij} + \lambda\|\hat{\mathbf{S}}\|_F^2, \\ &\text{s.t. } \hat{\mathbf{S}} \geq 0, \mathbf{1}^{\top}\hat{\mathbf{S}} = \mathbf{1}. \end{aligned} \tag{8}$$

The ultimate clustering result is generated by performing spectral clustering on the refined similarity matrix $\hat{\mathbf{S}}$, and the overall procedure is detailed in Algorithm (1).

3.5 Optimization

The optimization problem in Eq. (6) can be solved using alternating optimization methods, where in each iteration, one variable is fixed while the others are optimized, and this process continues iteratively until the objective function converges.

Update $\mathbf{W}^{(p)}$ with $\mathbf{S}$ and $\boldsymbol{\alpha}$ fixed. Fixing other variables, the subproblem concerning $\mathbf{W}^{(p)}$ can be rewritten as:

$$\begin{aligned} &\min_{\mathbf{W}^{(p)}} \sum_{p=1}^{V} \|\mathbf{X}^{(p)} - \mathbf{X}^{(p)}\mathbf{W}^{(p)}\|_F^2 + \\ &\sum_{p=1}^{V} \alpha_p^2 \operatorname{Tr}\left(\mathbf{W}^{(p)\top}\mathbf{X}^{(p)\top}\mathbf{L}_S\mathbf{X}^{(p)}\mathbf{W}^{(p)}\right), \\ &\text{s.t. } \mathbf{W}^{(p)\top}\mathbf{W}^{(p)} = \mathbf{I}. \end{aligned} \tag{9}$$

By removing irrelevant terms, we independently optimize $\mathbf{W}^{(p)}$ on each view as follows:

$$\begin{aligned} &\min_{\mathbf{W}^{(p)}} \operatorname{Tr}\left(\mathbf{W}^{(p)\top}\mathbf{A}^{(p)}\mathbf{W}^{(p)} - 2\mathbf{X}^{(p)\top}\mathbf{X}^{(p)}\mathbf{W}^{(p)}\right), \\ &\text{s.t. } \mathbf{W}^{(p)\top}\mathbf{W}^{(p)} = \mathbf{I}, \end{aligned} \tag{10}$$

where $\mathbf{A}^{(p)} = \left(\mathbf{X}^{(p)\top}\mathbf{X}^{(p)} + \alpha_p^2\mathbf{X}^{(p)\top}\mathbf{L}_S\mathbf{X}^{(p)}\right)$. The above equation can be relaxed as follows,

$$\begin{aligned} &\max_{\mathbf{W}^{(p)}} \operatorname{Tr}\left(\mathbf{W}^{(p)\top}\left(\gamma_{max}\mathbf{I} - \mathbf{A}^{(p)}\right)\mathbf{W}^{(p)} + 2\mathbf{X}^{(p)\top}\mathbf{X}^{(p)}\mathbf{W}^{(p)}\right), \\ &\text{s.t. } \mathbf{W}^{(p)\top}\mathbf{W}^{(p)} = \mathbf{I}, \end{aligned} \tag{11}$$

where γ_{max} is the largest eigenvalue of $\mathbf{A}^{(p)}$. According to reference [34], Eq. (11) can be solved by optimizing the following problem iteratively,

$$\begin{aligned} &\max_{\mathbf{W}^{(p)}} \operatorname{Tr}\left(\mathbf{W}^{(p)\top}\mathbf{B}^{(p)}\right), \\ &\text{s.t. } \mathbf{W}^{(p)\top}\mathbf{W}^{(p)} = \mathbf{I}, \end{aligned} \tag{12}$$

where $\mathbf{B}^{(p)} = 2\left(\gamma_{max}\mathbf{I} - \mathbf{A}^{(p)}\right)\mathbf{W}^{(p)*} + 2\mathbf{X}^{(p)\top}\mathbf{X}^{(p)}$ and $\mathbf{W}^{(p)*}$ denotes the optimal $\mathbf{W}^{(p)}$ in the last iteration. By performing SVD decomposition $\mathbf{B}^{(p)} = \mathbf{U}^{\top}\Sigma\mathbf{V}$, the optimal $\mathbf{W}^{(p)}$ at each iteration is $\mathbf{U}^{\top}\mathbf{V}$.

Update $\mathbf{S}$ with $\mathbf{W}^{(p)}$ and $\boldsymbol{\alpha}$ fixed. Fixing other variables, the subproblem concerning $\mathbf{S}$ can be rewritten as:

$$\begin{aligned} &\min_{\mathbf{S}} \sum_{p=1}^{V} \alpha_p^2 \operatorname{Tr}\left(\mathbf{W}^{(p)\top}\mathbf{X}^{(p)\top}\mathbf{L}_S\mathbf{X}^{(p)}\mathbf{W}^{(p)}\right) + \lambda\|\mathbf{S}\|_F^2, \\ &\text{s.t. } \mathbf{S} \geq 0, \mathbf{1}^{\top}\mathbf{S} = \mathbf{1}. \end{aligned} \tag{13}$$

The above function can be rewritten as follows,

$$\begin{aligned} &\min_{\mathbf{s}_{ij}} \sum_{p=1}^{V}\sum_{i,j=1}^{n} \frac{1}{2}\alpha_p^2\|\mathbf{x}_{i,:}^{(p)}\mathbf{W}^{(p)} - \mathbf{x}_{j,:}^{(p)}\mathbf{W}^{(p)}\|_2^2 s_{ij} + \lambda s_{ij}^2, \\ &\text{s.t. } s_{ij} \geq 0, \sum_{j=1}^{n} s_{ij} = 1. \end{aligned} \tag{14}$$

Considering that each column of $\mathbf{S}$ is uncorrelated with each other. Denoting $\mathbf{s}_{:,j}$ as a vector with s_{ij} to be the j-th element, Eq. (14) can be optimized in column form as follows,

$$\min_{\mathbf{s}_{:,j}} \frac{1}{2}\lambda\mathbf{s}_{:,j}^{\top}\mathbf{s}_{:,j} + \mathbf{e}_{:,j}^{\top}\mathbf{s}_{:,j}, s.t. \mathbf{s}_i \geq 0, \mathbf{s}_i{}^{\top}\mathbf{1} = 1, \tag{15}$$

where $\mathbf{e}_{i,j} = \frac{1}{4\lambda}\sum_{p=1}^{v}\alpha_p{}^2\|\mathbf{x}_{i,:}^{(p)}\mathbf{W}^{(p)} - \mathbf{x}_{j,:}^{(p)}\mathbf{W}^{(p)}\|_2^2$. Following [34], we can easily get the closed form solution of each $\mathbf{s}_i^{(p)}$.

Update $\boldsymbol{\alpha}$ with $\mathbf{W}^{(p)}$ and S fixed. Fixing other variables, the objective function with respect to $\boldsymbol{\alpha}$ can be formulated as

$$\min_{\boldsymbol{\alpha}} \sum_{p=1}^{v} \alpha_p^2 \mathbf{g}_p, s.t. \boldsymbol{\alpha}^\top \mathbf{1} = 1, \boldsymbol{\alpha} \geq 0, \tag{16}$$

where $\mathbf{g}_p = \mathrm{Tr}\left(\mathbf{W}^{(p)\top}\mathbf{X}^{(p)\top}\mathbf{L}_S\mathbf{X}^{(p)}\mathbf{W}^{(p)}\right)$. We can obtain the optimal α_p by Cauchy-Buniakowsky-Schwarz inequality as

$$\alpha_p = \frac{\frac{1}{\mathbf{g}_p}}{\sum_{p=1}^{v} \frac{1}{\mathbf{g}_p}}. \tag{17}$$

3.6 Discussion

Time complexity analysis. The time complexity of our proposed RAM-MVC is $O(\sum_{p=1}^{v} n^2 d_v + \sum_{p=1}^{v} n d_v^2 \tau + \sum_{p=1}^{v} d_v^3 \tau)$, where τ represents the number of iterations in Algorithm 2. Specifically, updating $\mathbf{W}^{(p)}$ costs $O(n^2 d_v + n d_v^2 \tau + d_v^3 \tau)$ totally. Calculating $\mathbf{A}^{(p)}$ needs $O(n^2 d_v)$ and performing matrix multiplication in each iteration of Algorithm 2 needs $O(n d_v^2 + d_v^3)$. The computational complexity of optimizing S is $O(\sum_{p=1}^{v} n^2 d_v)$ for matrix multiplication and $O(n^2)$ for solving Eq. (15). Updating $\boldsymbol{\alpha}$ costs $O(\sum_{p=1}^{v} n^2 d_v)$ for calculating $\mathbf{g}_p$.

Space complexity analysis. The main matrix variables required to be stored during the computation process of RAM-MVC include the raw data matrix $\{\mathbf{X}^{(p)}\}_{p=1}^{v}$, the imputation guidance matrix $\{\mathbf{H}^{(p)}\}_{p=1}^{v}$, the feature transformation matrix $\{\mathbf{W}^{(p)}\}_{p=1}^{v}$, the similarity matrix S, and the Laplacian matrix $\mathbf{L}_S$. Without considering the space occupied by vectors, the space complexity of RAM-MVC is $O(n^2 + \sum_{p=1}^{v}(n d_v + d_v^2))$.

4 EXPERIMENTS

4.1 Experimental Settings

Benchmark Datasets. Through investigation [19, 27], we find that single-cell multi-view data naturally encompass both technical and real missing events. Therefore, in this study, we have chosen to evaluate our model in a biomedical scenario. Six real-world single-cell multi-view datasets are involved: BMNC-I, BMNC-II, PBMC, SLN111, SMAGE-I, and SMAGE-II. Detailed information about these datasets is provided in Table 2. The BMNC dataset was sourced from the GEO database, which is a comprehensive archive of high-throughput gene expression data and genomic information [3]. The PBMC, SMAGE-3K, and SMAGE-10K datasets were obtained from the renowned biological database at www.10xgenomics.com. SLN111 originates from the work of Yosef et al. [31].

Competitive Algorithms. We compare the proposed RAM-MVC with the following state-of-the-art approaches, i.e., FMCNOF (Fast Multi-View Clustering via Nonnegative and Orthogonal Factorization) [47]; FastMICE (Fast Multi-View Clustering Via Ensembles: Towards Scalability, Superiority, and Simplicity) [14]; RMKM (Multi-View K-Means Clustering on Big Data) [4]; UOMVSC (Unified One-Step Multi-View Spectral Clustering) [37]; AMGL (Parameter-Free Auto-Weighted Multiple Graph Learning: A Framework for Multi-view Clustering and Semi-Supervised Classification) [32]; MSGL (Structured Graph Learning for Scalable Subspace Clustering: From Single View to Multiview.) [15]; DCCA (Deep cross-omics cycle attention model for joint analysis of single-cell multi-omics data) [59]; scMDC (Clustering of single-cell multi-omics data with a multimodal deep learning method) [24]; scMVAE (Deep-joint-learning analysis model of single cell transcriptome and open chromatin accessibility data) [58].

Table 2: Attribute-missing multi-view datasets in our experiments

Dataset	Size	Views	Clusters	Dimensions
BMNC-I	1728	2	5	1000/25
BMNC-II	1963	2	4	1000/25
PBMC	3762	2	16	1000/49
SLN111	6018	2	10	1000/112
SMAGE-I	2585	2	14	2000/2000
SMAGE-II	11020	2	12	2000/2000

Evaluation Metrics. In this study, we focus on the accuracy of clustering results. Consequently, four widely used external clustering evaluation metrics are employed: Accuracy (ACC), Normalized Mutual Information (NMI), Purity, and Adjusted Rand Index (ARI).

Training Settings. For all competitive algorithms, searches were conducted within the recommended parameter space to select the parameter combinations for optimal clustering performance. In our study, the λ parameter values were set to $[1, 10, 100, 1000]$, while the threshold t values were set to $[0.1, 0.3, 0.5, 0.7, 0.9]$. The experiments were repeated multiple times to accurately determine both the mean and the standard deviation. All trials were conducted on a Linux workstation equipped with an Intel Core i9-12900KF CPU and 64GB of RAM.

4.2 Performance Comparison

Table 3 presents the clustering performance of the RAM-MVC algorithm alongside nine baseline methods across six benchmark datasets. It is evident that RAM-MVC consistently achieves the optimal scores in most cases. In a total of 24 comparisons, RAM-MVC won first place in 58.33% of cases and was placed in the top two in 91.67% of instances. For datasets comprising over 10,000 instances, such as SMAGE-II, the RAM-MVC algorithm demonstrated superior performance relative to the average score, with an increase of (26.1%, 12.68%, 12.52%, 29.04%) in the ACC, NMI, Purity, and ARI metrics, respectively. For small datasets, such as BMNC-I and BMNC-II, in comparison with the average score, the RAM-MVC algorithm maintained its superior performance over comparative algorithms, with improvements in the four metrics (29.7%, 24.73%, 17.45%, 39.93%) and (23.5%, 26.39%, 16.66%, 31.5%), respectively. This observation highlights the RAM-MVC algorithm's consistent excellence across datasets of varying sizes. Moreover, it was found that underperformance occurs exclusively in the Purity metric. In analyzing the potential causes, the hypothesis is that class imbalance might be the underlying issue. For instance, assigning all instances to a single cluster results in a Purity value of 1; yet, this outcome does not equate to effective clustering. In terms of running time, our method does not offer a significant advantage. The comparison of running times of different models is detailed in Table 4.

Table 3: Clustering performance on six benchmark datasets, the top 2 scores highlighted in bold.

Methods	FMCNOF	FastMICE	RMKM	UOMVSC	AMGL	MSGL	DCCA	scMDC	scMVAE	RAM-MVC
					ACC(%)					
BMNC-I	53.41±0.00	**78.62±2.25**	61.81±0.00	72.97±0.00	21.68±0.09	70.62±10.99	71.30±0.00	68.55±2.11	65.42±0.09	**92.41±0.03**
BMNC-II	66.02±0.00	94.95±5.48	61.90±0.00	98.42±0.00	26.08±0.13	91.61±7.14	**98.93± 0.00**	79.54±1.14	63.73±0.00	**99.19±0.00**
PBMC	35.83±0.00	66.23±1.74	**71.32±0.00**	70.79±0.00	8.50±0.11	65.39±2.85	64.49±0.00	70.85±3.39	61.35±0.00	**71.16 ±0.51**
SLN111	56.23±0.00	49.23±4.06	53.77±0.00	**81.11±0.00**	11.65±0.29	51.73±5.51	52.43±0.00	64.70±6.25	52.88±2.70	**84.96±0.66**
SMAGE-I	43.98±0.00	47.93±1.70	62.44±0.00	61.59±0.00	9.32±0.17	55.53±2.57	48.78±0.00	**65.62±1.88**	45.69±0.00	**70.75±0.15**
SMAGE-II	67.35±0.00	50.53±3.14	57.85±0.00	**80.26±0.00**	9.36±0.10	53.08±2.24	47.21±0.00	58.32±1.35	42.98±0.00	**77.98±0.03**
					NMI(%)					
BMNC-I	50.29±0.00	**75.60±1.38**	56.33±0.00	73.61±0.00	32.00±0.03	69.05±6.67	60.35±0.00	74.70±0.29	68.19±0.53	**86.97±0.05**
BMNC-II	55.47±0.00	75.93±1.16	70.79±0.00	93.11±0.00	0.30±0.01	84.90±5.82	**94.74±0.00**	74.80±1.79	71.83±0.00	**95.49±0.00**
PBMC	44.04±0.00	70.19±1.15	69.63±0.00	**73.05±0.00**	1.30±0.04	66.58±1.41	70.25±0.00	72.30±1.36	68.50±0.00	**72.51 ±0.24**
SLN111	41.98±0.00	65.25±2.43	67.89±0.00	**79.33±0.00**	0.66±0.13	60.27±3.18	66.49±0.00	71.74±3.98	66.78±0.07	**81.14±0.60**
SMAGE-I	38.08±0.00	56.01±1.02	60.92±0.00	60.74±0.00	1.83±0.12	52.11±1.86	53.34±0.00	**61.76±0.81**	53.94±0.00	**62.05±0.16**
SMAGE-II	46.97±0.00	57.25±1.17	60.16±0.00	**68.73±0.00**	0.34±0.02	54.68±1.08	54.63±0.00	59.80±0.52	54.80±0.00	**63.50±0.08**
					Purity(%)					
BMNC–I	71.53±0.00	**91.13±0.61**	81.31±0.00	90.97±0.00	21.81±0.14	86.65±5.15	71.30±0.00	87.30±2.00	72.66±0.09	**92.41±0.03**
BMNC-II	77.99±0.00	91.26±5.83	92.56±0.00	98.42±0.00	26.18±0.14	95.31±2.37	**98.93±0.00**	92.10±0.15	70.05±0.00	**99.19±0.00**
PBMC	41.23±0.00	80.19±1.73	77.17±0.00	**81.63±0.00**	8.73±0.12	74.98±1.76	65.39±0.00	78.30±2.81	62.17±0.00	**80.80 ±0.18**
SLN111	56.23±0.00	85.39±1.31	85.66±0.00	**88.32±0.00**	11.77±0.32	79.04±1.74	56.46±0.00	84.50±5.15	56.09±3.47	**86.28±0.80**
SMAGE-I	65.49±0.00	77.94±0.67	**78.69±0.00**	78.34±0.00	9.59±0.16	71.11±1.73	50.83±0.00	**78.93±0.37**	48.63±0.00	72.69±0.07
SMAGE-II	72.59±0.00	82.28±0.97	**85.39±0.00**	**83.64±0.00**	9.41±0.10	78.92±0.30	51.51±0.00	82.86±0.22	46.58±0.00	78.43±0.03
					ARI(%)					
BMNC-I	31.62±0.00	**58.77±1.47**	44.11±0.00	55.39±0.00	0.04±0.03	49.89±10.95	49.34±0.00	55.19±1.51	45.62±0.18	**83.26±0.03**
BMNC-II	55.45±0.00	93.67±6.54	52.02±0.00	97.36±0.00	0.06±0.01	86.61±4.37	**97.93±0.00**	62.44±4.18	52.62±0.00	**97.96±0.00**
PBMC	19.09±0.00	56.13±2.13	59.10±0.00	**60.22±0.00**	0.01±0.02	53.12±2.05	55.10±0.00	59.79±4.56	51.95±0.00	**60.90 ±0.56**
SLN111	28.42±0.00	41.50±4.52	43.82±0.00	**81.98±0.00**	0.05±0.05	40.99±7.48	45.50±0.00	55.79±9.04	45.61±2.09	**84.40±0.76**
SMAGE-I	29.56±0.00	32.44±1.65	47.11±0.00	49.57±0.00	0.02±0.02	38.77±3.28	38.17±0.00	**52.02±1.28**	30.08±0.00	**57.52±0.38**
SMAGE-II	50.52±0.00	37.38±2.97	45.57±0.00	**74.24±0.00**	0.01±0.00	41.23±3.19	38.81±0.00	46.52±2.57	29.59±0.00	**69.47±0.05**

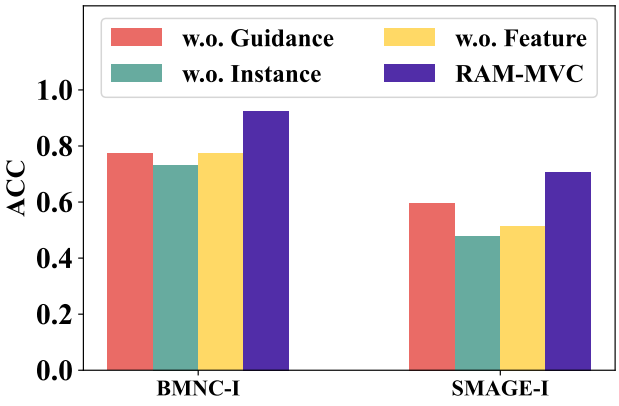

Figure 3: The ablation study was conducted on the proposed three variants: 1) w.o. Feature, 2) w.o. Instance, and 3) w.o. Guidance across the BMNC-I and SMAGE-I datasets, visualized using ACC metrics. (w.o. denotes without).

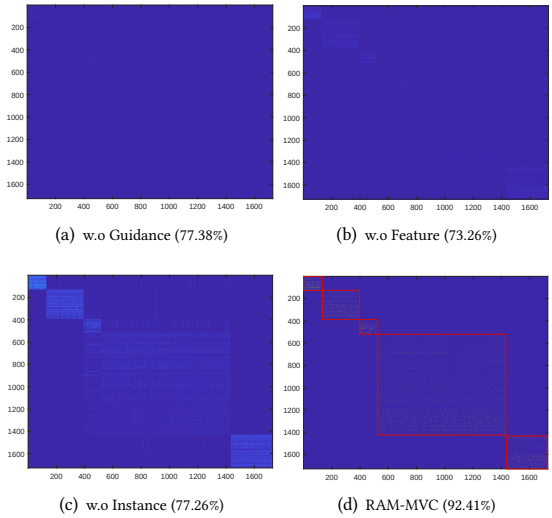

(a) w.o Guidance (77.38%) (b) w.o Feature (73.26%)

(c) w.o Instance (77.26%) (d) RAM-MVC (92.41%)

Figure 4: Illustrations of learned similarity matrix on BMNC-I datasets.

Table 4: The comparison of running times (s) of different algorithms

Datasets	BMNC-I	BMNC-II	PBMC	SLN111	SMAGE-I	SMAGE-II
FMCNOF	0.20	0.19	0.40	0.48	0.66	3.03
FastMICE	2.62	2.77	3.90	5.70	7.32	15.73
RMKM	2.53	2.89	10.97	22.06	13.25	84.67
UOMVSC	0.92	1.09	8.79	27.02	4.37	129.58
AMGL	15.87	22.14	178.73	1207.77	27.80	4203.80
MSGL	3.23	4.97	9.56	38.45	21.03	59.18
DCCA	16.58	10.87	23.80	61.44	47.65	110.92
scMDC	108.15	170.60	101.46	424.02	40.67	149.78
scMVAE	296.19	262.61	28.81	363.81	72.82	178.54
RAM-MVC	13.45	15.05	98.67	441.00	52.47	3731.20

4.3 Ablation Study

To evaluate the effectiveness of the proposed module, we constructed three variants of RAM-MVC as follows: (1) RAM-MVC w.o. Feature: The feature-level graph learning module was removed from the complete model; (2) RAM-MVC w.o. Instance: The instance-level graph learning module was removed from the complete model; (3) RAM-MVC w.o. Guidance: The reliable imputation guidance module was removed from the complete model.

Fig. 3 presents the results of ablation experiments on BMNC-I and SMAGE-I datasets. We found that the variant RAM-MVC w.o. Guidance experienced significant performance degradation across two datasets, illustrating that the proposed reliable guidance module effectively addresses the discriminative imputation issue, thereby enhancing the clustering performance. Additionally, removing the instance-level and feature-level learning modules significantly degrades the model's performance to varying degrees, which illustrates the effectiveness of the bi-level cooperative imputation module. Fig. 4 presents the similarity matrix corresponding to various variants, indicating that preserving all modules achieves the highest-quality similarity matrix. To summarize, the ablation experiments underscore the effectiveness of our proposed three modules and highlight the superiority of the unified clustering framework integrating reliable guidance and bi-level cooperative imputation.

4.4 Parameter Sensitivity and Convergence Analysis

According to the object function in Eq. (6), the regularization hyperparameter λ is incorporated, while the confidence threshold t is introduced in Eq. (2). Thus, the RAM-MVC model incorporates two hyperparameters: λ and t. To investigate the impact of hyperparameters on model performance, comprehensive parameter experiments were conducted on the BMNC-I and SMAGE-I datasets, the result is shown in Fig. 5. It is observed that across two datasets, fluctuations in λ significantly affect clustering performance, yet stability can be maintained within a certain range. This indicates that RAM-MVC is sensitive to the λ parameter, requiring adjustments within an appropriate range for optimal performance. Conversely, t does not exhibit the same level of sensitivity as λ. On the SMAGE-I dataset, the parameter t has a limited impact on the final performance. However, for the BMNC-I dataset, significant performance

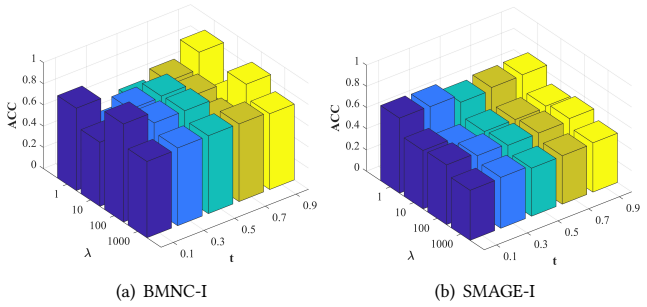

(a) BMNC-I (b) SMAGE-I

Figure 5: Parameter sensitive analysis of the proposed RAM-MVC on BMNC-I and SMAGE-I datasets.

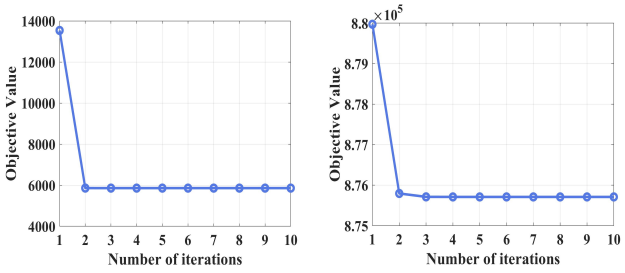

(a) BMNC-I (b) SMAGE-I

Figure 6: Objective function values at each iteration of the RAM-MVC on BMNC-I and SMAGE-I datasets.

fluctuations were observed, demonstrating that the sensitivity of the parameter t is related to the dataset's characteristics.

Furthermore, to investigate the convergence of RAM-MVC, convergence curves for the BMNC-I and SMAGE-I datasets were plotted, as depicted in Fig. 6. From the curves, it can be observed that the RAM-MVC algorithm converges after multiple iterations.

5 CONCLUSIONS

In summary, we propose a novel MVC method tailored for attribute-missing events, which overcomes the limitations of current methods that indiscriminately treat all missing attributes as zero values and neglect the contributions of bi-level structural information to feature reconstruction. The proposed RAM-MVC model seamlessly integrates reliable guidance and bi-level imputation into a unified learning framework. Instance-level and feature-level structural information is simultaneously leveraged to generate high-quality reconstructed features, and the confidence of zero values is calculated to facilitate discriminatory imputation on missing information, thereby avoiding over-interpolation. Furthermore, we have explored the application of this method in the biomedical field, demonstrating that it effectively completes the missing attribute information in single-cell multi-view data and achieves enhanced clustering performance. Experimental results from six real-world datasets underscore RAM-MVC's superiority over other benchmark methods.

REFERENCES

[1] Brian B Avants, Nicholas J Tustison, and James R Stone. 2021. Similarity-driven multi-view embeddings from high-dimensional biomedical data. *Nature computational science* 1, 2 (2021), 143–152.

[2] Md Bahadur Badsha, Rui Li, Boxiang Liu, Yang I Li, Min Xian, Nicholas E Banovich, and Audrey Qiuyan Fu. 2020. Imputation of single-cell gene expression with an autoencoder neural network. *Quantitative Biology* 8, 1 (2020), 78–94.

[3] Tanya Barrett, Tugba O Suzek, Dennis B Troup, Stephen E Wilhite, Wing-Chi Ngau, Pierre Ledoux, Dmitry Rudnev, Alex E Lash, Wataru Fujibuchi, and Ron Edgar. 2005. NCBI GEO: mining millions of expression profiles—database and tools. *Nucleic acids research* 33, suppl_1 (2005), D562–D566.

[4] Xiao Cai, Feiping Nie, and Heng Huang. 2013. Multi-view k-means clustering on big data. In *Twenty-Third International Joint conference on artificial intelligence*.

[5] Zhiwen Cao and Xijiong Xie. 2024. Multi-view unsupervised complementary feature selection with multi-order similarity learning. *Knowledge-Based Systems* 283 (2024), 111172.

[6] Guoqing Chao, Yi Jiang, and Dianhui Chu. 2024. Incomplete Contrastive Multi-View Clustering with High-Confidence Guiding. In *Proceedings of the AAAI Conference on Artificial Intelligence*, Vol. 38. 11221–11229.

[7] Zhe Chen, Xiao-Jun Wu, Tianyang Xu, and Josef Kittler. 2023. Fast self-guided multi-view subspace clustering. *IEEE transactions on image processing* (2023).

[8] Wanqiu Cui, Junping Du, Dawei Wang, Feifei Kou, and Zhe Xue. 2021. MVGAN: Multi-view graph attention network for social event detection. *ACM Transactions on Intelligent Systems and Technology (TIST)* 12, 3 (2021), 1–24.

[9] Xiaowen Dong, Pascal Frossard, Pierre Vandergheynst, and Nikolai Nefedov. 2012. Clustering with multi-layer graphs: A spectral perspective. *IEEE Transactions on Signal Processing* 60, 11 (2012), 5820–5831.

[10] Haitao Fu, Feng Huang, Xuan Liu, Yang Qiu, and Wen Zhang. 2022. MVGCN: data integration through multi-view graph convolutional network for predicting links in biomedical bipartite networks. *Bioinformatics* 38, 2 (2022), 426–434.

[11] Ellen Goeleven, Rudi De Raedt, Lemke Leyman, and Bruno Verschuere. 2008. The Karolinska directed emotional faces: a validation study. *Cognition and emotion* 22, 6 (2008), 1094–1118.

[12] Wenyu Hao, Shanmin Pang, Xiuxiu Bai, and Jianru Xue. 2023. Tensor-Based Incomplete Multi-View Clustering With Low-Rank Data Reconstruction and Consistency Guidance. *IEEE Transactions on Circuits and Systems for Video Technology* (2023).

[13] Yaru Hao, Xiao-Yuan Jing, Runhang Chen, and Wei Liu. 2023. Learning enhanced specific representations for multi-view feature learning. *Knowledge-Based Systems* 272 (2023), 110590.

[14] Dong Huang, Chang-Dong Wang, and Jian-Huang Lai. 2023. Fast multi-view clustering via ensembles: Towards scalability, superiority, and simplicity. *IEEE Transactions on Knowledge and Data Engineering* (2023).

[15] Zhao Kang, Zhiping Lin, Xiaofeng Zhu, and Wenbo Xu. 2021. Structured graph learning for scalable subspace clustering: From single view to multiview. *IEEE Transactions on Cybernetics* 52, 9 (2021), 8976–8986.

[16] Youngjune Lee, Yeongjong Jeong, Keunchan Park, and SeongKu Kang. 2023. MvFS: Multi-view Feature Selection for Recommender System. In *Proceedings of the 32nd ACM International Conference on Information and Knowledge Management*. 4048–4052.

[17] Feng Li, Yang Liu, Jinxing Liu, Daohui Ge, and Junliang Shang. 2024. A framework for scRNA-seq data clustering based on multi-view feature integration. *Biomedical Signal Processing and Control* 89 (2024), 105785.

[18] Lusi Li, Zhiqiang Wan, and Haibo He. 2021. Incomplete multi-view clustering with joint partition and graph learning. *IEEE Transactions on Knowledge and Data Engineering* 35, 1 (2021), 589–602.

[19] Wei Vivian Li and Jingyi Jessica Li. 2018. An accurate and robust imputation method scImpute for single-cell RNA-seq data. *Nature communications* 9, 1 (2018), 997.

[20] Xingfeng Li, Yinghui Sun, Quansen Sun, Jia Dai, and Zhenwen Ren. 2023. Distribution Consistency based Fast Anchor Imputation for Incomplete Multi-view Clustering. In *Proceedings of the 31st ACM International Conference on Multimedia*. 368–376.

[21] Xiang-Long Li, Man-Sheng Chen, Chang-Dong Wang, and Jian-Huang Lai. 2022. Refining graph structure for incomplete multi-view clustering. *IEEE transactions on neural networks and learning systems* (2022).

[22] Yifeng Li, Fang-Xiang Wu, and Alioune Ngom. 2018. A review on machine learning principles for multi-view biological data integration. *Briefings in bioinformatics* 19, 2 (2018), 325–340.

[23] Naiyao Liang, Zuyuan Yang, and Shengli Xie. 2022. Incomplete multi-view clustering with sample-level auto-weighted graph fusion. *IEEE Transactions on Knowledge and Data Engineering* 35, 6 (2022), 6504–6511.

[24] Xiang Lin, Tian Tian, Zhi Wei, and Hakon Hakonarson. 2022. Clustering of single-cell multi-omics data with a multimodal deep learning method. *Nature communications* 13, 1 (2022), 7705.

[25] Yijie Lin, Yuanbiao Gou, Zitao Liu, Boyun Li, Jiancheng Lv, and Xi Peng. 2021. Completer: Incomplete multi-view clustering via contrastive prediction. In *Proceedings of the IEEE/CVF conference on computer vision and pattern recognition*. 11174–11183.

[26] Zerun Lin and Le Ou-Yang. 2023. Inferring gene regulatory networks from single-cell gene expression data via deep multi-view contrastive learning. *Briefings in Bioinformatics* 24, 1 (2023), bbac586.

[27] George C Linderman, Jun Zhao, Manolis Roulis, Piotr Bielecki, Richard A Flavell, Boaz Nadler, and Yuval Kluger. 2022. Zero-preserving imputation of single-cell RNA-seq data. *Nature communications* 13, 1 (2022), 192.

[28] Cheng Liu, Si Wu, Rui Li, Dazhi Jiang, and Hau-San Wong. 2023. Self-supervised graph completion for incomplete multi-view clustering. *IEEE Transactions on Knowledge and Data Engineering* (2023).

[29] Suyuan Liu, Junpu Zhang, Yi Wen, Xihong Yang, Siwei Wang, Yi Zhang, En Zhu, Chang Tang, Long Zhao, and Xinwang Liu. 2024. Sample-Level Cross-View Similarity Learning for Incomplete Multi-View Clustering. In *Proceedings of the AAAI Conference on Artificial Intelligence*, Vol. 38. 14017–14025.

[30] Zihuan Liu, Tong Liu, Wenke Sun, Yongzhong Zhao, and Xiaodi Wang. 2022. M-band wavelet-based imputation of scRNA-seq matrix and multi-view clustering of cell. *bioRxiv* (2022), 2022–12.

[31] Romain Lopez, Jeffrey Regier, Michael B Cole, Michael I Jordan, and Nir Yosef. 2018. Deep generative modeling for single-cell transcriptomics. *Nature methods* 15, 12 (2018), 1053–1058.

[32] Feiping Nie, Jing Li, Xuelong Li, et al. 2016. Parameter-free auto-weighted multiple graph learning: a framework for multiview clustering and semi-supervised classification.. In *IJCAI*, Vol. 9. 1881–1887.

[33] Feiping Nie, Zhenyu Ma, Jingyu Wang, and Xuelong Li. 2023. Fast sparse discriminative k-means for unsupervised feature selection. *IEEE Transactions on Neural Networks and Learning Systems* (2023).

[34] Feiping Nie, Xiaoqian Wang, and Heng Huang. 2014. Clustering and projected clustering with adaptive neighbors. In *Proceedings of the 20th ACM SIGKDD international conference on Knowledge discovery and data mining*. 977–986.

[35] Xin Peng, Jieren Cheng, Xiangyan Tang, Bin Zhang, and Wenxuan Tu. 2024. Multi-view graph imputation network. *Information Fusion* 102 (2024), 102024.

[36] Jingyu Pu, Chenhang Cui, Xinyue Chen, Yazhou Ren, Xiaorong Pu, Zhifeng Hao, S Yu Philip, and Lifang He. 2024. Adaptive Feature Imputation with Latent Graph for Deep Incomplete Multi-View Clustering. In *Proceedings of the AAAI Conference on Artificial Intelligence*, Vol. 38. 14633–14641.

[37] Chang Tang, Zhenglai Li, Jun Wang, Xinwang Liu, Wei Zhang, and En Zhu. 2022. Unified one-step multi-view spectral clustering. *IEEE Transactions on Knowledge and Data Engineering* 35, 6 (2022), 6449–6460.

[38] Chang Tang, Xiao Zheng, Xinwang Liu, Wei Zhang, Jing Zhang, Jian Xiong, and Lizhe Wang. 2021. Cross-view locality preserved diversity and consensus learning for multi-view unsupervised feature selection. *IEEE Transactions on Knowledge and Data Engineering* 34, 10 (2021), 4705–4716.

[39] Huayi Tang and Yong Liu. 2022. Deep safe incomplete multi-view clustering: Theorem and algorithm. In *International Conference on Machine Learning*. PMLR, 21090–21110.

[40] Zhiqiang Tao, Hongfu Liu, Huazhu Fu, and Yun Fu. 2019. Multi-view saliency-guided clustering for image cosegmentation. *IEEE Transactions on Image Processing* 28, 9 (2019), 4634–4645.

[41] Menghan Wang, Yujie Lin, Guli Lin, Keping Yang, and Xiao-ming Wu. 2020. M2GRL: A multi-task multi-view graph representation learning framework for web-scale recommender systems. In *Proceedings of the 26th ACM SIGKDD international conference on knowledge discovery & data mining*. 2349–2358.

[42] Yiming Wang, Dongxia Chang, Zhiqiang Fu, Jie Wen, and Yao Zhao. 2022. Incomplete multiview clustering via cross-view relation transfer. *IEEE Transactions on Circuits and Systems for Video Technology* 33, 1 (2022), 367–378.

[43] Jie Wen, Zheng Zhang, Zhao Zhang, Lei Zhu, Lunke Fei, Bob Zhang, and Yong Xu. 2021. Unified tensor framework for incomplete multi-view clustering and missing-view inferring. In *Proceedings of the AAAI conference on artificial intelligence*, Vol. 35. 10273–10281.

[44] Yangyang Wu, Xiaoye Miao, Xinyu Huang, and Jianwei Yin. 2023. Jointly imputing multi-view data with optimal transport. In *Proceedings of the AAAI Conference on Artificial Intelligence*, Vol. 37. 4747–4755.

[45] Shiting Xiao, Yufu Wang, Ammon Perkes, Bernd Pfrommer, Marc Schmidt, Kostas Daniilidis, and Marc Badger. 2023. Multi-view tracking, re-id, and social network analysis of a flock of visually similar birds in an outdoor aviary. *International Journal of Computer Vision* 131, 6 (2023), 1532–1549.

[46] Gehui Xu, Jie Wen, Chengliang Liu, Bing Hu, Yicheng Liu, Lunke Fei, and Wei Wang. 2024. Deep Variational Incomplete Multi-View Clustering: Exploring Shared Clustering Structures. In *Proceedings of the AAAI Conference on Artificial Intelligence*, Vol. 38. 16147–16155.

[47] Ben Yang, Xuetao Zhang, Feiping Nie, Fei Wang, Weizhong Yu, and Rong Wang. 2020. Fast multi-view clustering via nonnegative and orthogonal factorization. *IEEE Transactions on Image Processing* 30 (2020), 2575–2586.

[48] Liying Yang, Zhenwei Zhu, Xuxin Lin, Jian Nong, and Yanyan Liang. 2023. Long-Range Grouping Transformer for Multi-View 3D Reconstruction. In *Proceedings*

of the IEEE/CVF International Conference on Computer Vision. 18257–18267.

[49] Mouxing Yang, Yunfan Li, Peng Hu, Jinfeng Bai, Jiancheng Lv, and Xi Peng. 2022. Robust multi-view clustering with incomplete information. *IEEE Transactions on Pattern Analysis and Machine Intelligence* 45, 1 (2022), 1055–1069.

[50] Xihong Yang, Jin Jiaqi, Siwei Wang, Ke Liang, Yue Liu, Yi Wen, Suyuan Liu, Sihang Zhou, Xinwang Liu, and En Zhu. 2023. Dealmvc: Dual contrastive calibration for multi-view clustering. In *Proceedings of the 31st ACM International Conference on Multimedia*. 337–346.

[51] Fangchen Yu, Zhan Shi, Yuqi Ma, Jianfeng Mao, and Wenye Li. 2023. From Incompleteness to Unity: A Framework for Multi-view Clustering with Missing Values. In *International Conference on Neural Information Processing*. Springer, 101–112.

[52] Haoliang Yuan, Junyu Li, Yong Liang, and Yuan Yan Tang. 2022. Multi-view unsupervised feature selection with tensor low-rank minimization. *Neurocomputing* 487 (2022), 75–85.

[53] Chao Zhang, Huaxiong Li, Wei Lv, Zizheng Huang, Yang Gao, and Chunlin Chen. 2023. Enhanced tensor low-rank and sparse representation recovery for incomplete multi-view clustering. In *Proceedings of the AAAI Conference on Artificial Intelligence*, Vol. 37. 11174–11182.

[54] Rui Zhang, Yunxing Zhang, and Xuelong Li. 2020. Unsupervised feature selection via adaptive graph learning and constraint. *IEEE Transactions on neural networks and learning systems* 33, 3 (2020), 1355–1362.

[55] Wei Zhang, Zhaohong Deng, Te Zhang, Kup-Sze Choi, Jun Wang, and Shitong Wang. 2021. Incomplete multiple view fuzzy inference system with missing view imputation and cooperative learning. *IEEE Transactions on Fuzzy Systems* 30, 8 (2021), 3038–3051.

[56] Zhenwei Zhu, Liying Yang, Ning Li, Chaohao Jiang, and Yanyan Liang. 2023. Umiformer: Mining the correlations between similar tokens for multi-view 3d reconstruction. In *Proceedings of the IEEE/CVF International Conference on Computer Vision*. 18226–18235.

[57] Ruohan Zong, Yang Zhang, Lanyu Shang, and Dong Wang. 2023. Contrastfaux: Sparse semi-supervised fauxtography detection on the web using multi-view contrastive learning. In *Proceedings of the ACM Web Conference 2023*. 3994–4003.

[58] Chunman Zuo and Luonan Chen. 2021. Deep-joint-learning analysis model of single cell transcriptome and open chromatin accessibility data. *Briefings in Bioinformatics* 22, 4 (2021), bbaa287.

[59] Chunman Zuo, Hao Dai, and Luonan Chen. 2021. Deep cross-omics cycle attention model for joint analysis of single-cell multi-omics data. *Bioinformatics* 37, 22 (2021), 4091–4099.